

Accretion disk's magnetic field controlled the composition of the terrestrial planets

William F. McDonough^{*1,2,3} and Takashi Yoshizaki²

¹Department of Geology, University of Maryland, College Park, MD
20742, USA

²Department of Earth Science, Graduate School of Science, Tohoku
University, Sendai, Miyagi 980-8578, Japan

³Research Center of Neutrino Sciences, Tohoku University, Sendai,
Miyagi 980-8578, Japan

March 17, 2024

Chondrites, the building blocks of the terrestrial planets, have mass and atomic proportions of oxygen, iron, magnesium, and silicon totaling $\geq 90\%$ and variable Mg/Si ($\sim 25\%$), Fe/Si (factor of ≥ 2), and Fe/O (factor of ≥ 3). The Earth and terrestrial planets (Mercury, Venus, and Mars) are differentiated into three layers: a metallic core, a silicate shell (mantle and crust), and a volatile envelope of gases, ices, and, for the Earth, liquid water. Each layer has different dominant elements (e.g., increasing Fe content with depth and increasing oxygen content to the surface). What remains unknown is to what degree did physical processes during nebular disk accretion versus those during post-nebular disk accretion (e.g., impact erosion) influ-

^{*}Corresponding author. E-mail: mcdonoug@umd.edu

ence these final bulk compositions. Here we predict terrestrial planet compositions and show that their core mass fractions and uncompressed densities correlate with their heliocentric distance, and follow a simple model of the magnetic field strength in the protoplanetary disk. Our model assesses the distribution of iron in terms of increasing oxidation state, aerodynamics, and a decreasing magnetic field strength outward from the Sun, leading to decreasing core size of the terrestrial planets with radial distance. This distribution would enhance habitability in our solar system, and would be equally applicable to exo-planetary systems.

The formation of metallic cores in terrestrial planets greatly influences the thermal and biological evolution of a planet. Core formation concentrates the heat producing elements (i.e., potassium, thorium and uranium) into the insulating, outer silicate shell and produces a conductive fluid, which can create a planetary magnetic field. The mass fraction of metallic core in Mercury, Venus, Earth, and Mars decreases with heliocentric distance from about 2/3, to 1/3 (Venus and Earth), to 1/5, respectively (Sohl and Schubert, 2015). What chemical and/or physical process produced the large variation observed in Fe/O values in chondrites and the terrestrial planets, particularly for Mercury? The presence of a long-lived, internally convecting metallic core results in dynamo action and the generation of a planet's surrounding protective magnetosphere that nurtures life. These differentiated planets represent the most likely home for life and its evolution.

The compositions of the terrestrial planets and chondritic asteroids record, on average, an outward increase in oxygen fugacity, potentially a decrease in the nebular condensation temperature, and decreasing amounts of metallic iron contributing to planet building. The redox and temperature gradients leads to less metallic iron and more H- and O-rich solids

(i.e., phyllosilicates) outward in the solar system. Importantly, nebular condensates do not reach the high Fe/Si values of Mercury even with strongly reduced, high-temperature conditions (Ebel and Alexander, 2011). Thus, further metal-oxide separation processes are needed.

Compositional models for the terrestrial planets are constructed from the following data sets: composition of the Sun (i.e., >99% mass of the solar system), chemical trends for samples from a planet, satellite observations, and compositions of chondritic meteorites (i.e., the solar system's building blocks of undifferentiated rock and metal mixtures). Importantly, the chondrites that we have, however, are those leftover from planet building. Here we use our earlier compositional models for the Earth (McDonough, 2014) and Mars (Yoshizaki and McDonough, 2020b) and model the recent data from the MESSENGER mission to Mercury to predict its bulk composition (Table 1), which is consistent with known physical and chemical constraints (Methods). Given limited data for Venus, which is consistent with an Earth-like analog (Surkov et al., 1987; Dumoulin et al., 2017), we assume it has a bulk Earth composition.

Chondrites are geologically unprocessed materials, with their chemical compositions reflecting the local nebular conditions. However, chondrites differ markedly in their redox states and major element compositions (Figures 1 and 2). The redox state, mineralogies, and isotopic compositions of chondrites and other meteorites demonstrate that the early solar system was not compositionally homogeneous (Warren, 2011). Significantly, the less oxidized Non-Carbonaceous (NC) meteorites, including the enstatite and ordinary chondrites (Figure 2), are viewed as coming from inner solar system regions closer to the Sun (i.e., mostly 2 to 3 AU) than the oxidized Carbonaceous Chondrites (CC) and related

meteorites (Kruijer et al., 2017). The redox state and a dozen or so isotopic systems now link enstatite chondrites and Earth and equally, ordinary chondrites and Mars (Warren, 2011).

The Fe content of chondrites typically ranges from 1/5 to $<1/3$ of their total mass, with atomic Fe/Si typically 0.74 ± 0.12 , whereas some rare chondrite groups (i.e., CB, CH, and G types) can have Fe/Si values up to 8 (Figure 2b). The amount of iron accreted by a chondritic or terrestrial planet is not set by any particular rule; in the nebula, condensing iron-nickel grains, and other metallic alloys, are distinctly influenced by aerodynamic, gravitational, photophoretic, and electromagnetic sorting forces, compared to silicates (Weidenschilling, 1978; Wurm et al., 2013; Kruss and Wurm, 2018).

A planet's mass fraction of core to silicate shell reflects the accretion disk's average local redox state, accretion proportions of metal relative to silicates, and the redox conditions accompanying core-mantle differentiation. Impact-induced erosion/evaporation can also modify the mass fraction of core. Accretion sets the planetary values of Fe/O, Fe/Si, and Fe/Mg, which accounts for $\sim 93\%$ of its mass, with the addition of the minor elements, Ca, Al, Ni, and S, bringing the total to 99 wt% (Figure 1). A planet's mantle Mg# (i.e., atomic $\text{Mg}/(\text{Mg}+\text{Fe})$), therefore, is the recorder of the average redox state that accompanied core-mantle differentiation.

Mercury has the largest metallic core, high Fe/Al (21.8) and Mg/Si (1.4) values (Table 1 and Figure 2) and a silicate sphere with negligible Fe (i.e., Mg# ~ 0.99) (Nittler et al., 2018). By comparison, Mars has a smaller metallic core, a lower atomic Fe/Al (7.3) and Mg/Si (1.02) and a silicate shell with a low Mg# (0.79) than Earth (9.7, 1.11, and

0.89, respectively) (Table 1). Therefore, the silicate shells of Mars, Earth (and Venus), and Mercury get progressively relatively smaller, their cores relatively bigger, and their mantles more Mg#-rich with heliocentric distance.

Importantly, we show that the mean atomic number of the terrestrial planets increases inwards and show a correlation between heliocentric distance and a planet's uncompressed density (Figure 3). This planetary density trend also extends to bodies in the asteroidal belt: undifferentiated and differentiated asteroids are less dense than the terrestrial planets (Figure 3). Most chondrites have sub-solar Fe/Si (Figure 2b) and show a marked variation in Fe/Si and metallic iron content. Thus, the outward decrease of planetary density appears to primarily reflect dynamic metal-oxide separation in the protoplanetary disk, rather than post-accretionary processes.

Many processes can lead to chemical segregation in a protoplanetary disk, including aerodynamic sorting of metal and oxide (Weidenschilling, 1978), and electromagnetic separation of magnetized micro-particles of Fe-Ni alloys (existing below their Curie point with a stable magnetic spin) from silicates (Harris and Tozer, 1967; Larimer and Anders, 1970). Metal-oxide separation during chondrule formation might also be an effective separation process (Connolly et al., 2001). Recently, Wurm et al. (Wurm et al., 2013) also observed that photophoretic separation enhances metal-silicate fractionation. Thus, various physical sorting mechanisms in the nebular likely established the variation in Fe/O, Fe/Si, and Fe/Mg in chondrites and terrestrial planets. The degree of inward enrichment of magnetic micro-particles in the protoplanetary disk appears to scale radially with its magnetic field strength.

We show a correlation between the metallic core fraction and heliocentric distance for the terrestrial planets (Figure 3). This trend is interpreted as resulting from a decay of magnetic field strength in the protoplanetary disk and is consistent with paleomagnetic intensities recorded in meteorites (Bryson et al., 2020; Fu et al., 2020), magneto-hydrodynamic (MHD) disk models (Bai, 2015), and a simple Biot-Savart law that describes a 3D radial dependent magnetic field strength:

$$B = \frac{\mu_0 I}{2\pi r} \quad (1)$$

where B is magnetic flux density (Tesla, or $\text{kg s}^{-2} \text{A}^{-1}$), μ_0 is the magnetic constant (H m^{-1} or N A^{-2}), I is current (A), r is position in 3D-space (m) (Methods and Supplementary Figure 1). Azimuthal magnetic fields are likely to be strongest in the midplane (Wardle, 2007), the site of planetary accretion. The magnetic field strength of protoplanetary disk is recognized as a constantly evolving 4 dimensional phenomena that have been extensively treated by sophisticated MHD modeling (e.g., (Wardle, 2007)). Our perspective simply takes as a set of average conditions for the midplane of the disk at 4 critical distances: Mercury ($500 \mu\text{T}$, assumes a saturation field (Levy, 1978)), Earth ($100 \mu\text{T}$ (Wardle, 2007)), and Vesta ($\sim 50 \mu\text{T}$ (Wang et al., 2017)), with interpolations for Mars ($60 \mu\text{T}$). This simple model (Figure 1) appeals to a fundamental scaling relationship ($B \propto r^{-1.3}$) that views the magnetic field strength at the disk's midplane decreasing with distance from the central current moment of the evolving Sun. MHD modeling predicts $B \propto r^{-1.6}$ (Wardle, 2007; Bai, 2015). With mT magnetic field strength of the disk at $\sim 1 \text{ AU}$ is approximately sub-equal in its horizontal and vertical components and increases significantly towards the disk's center (Wardle, 2007). Kruss and Wurm (Kruss and Wurm, 2018) suggested the enhanced growth of iron-rich planetesimals in the inner region of protoplanetary disks

leads to an iron gradient in the solar system. A corollary of this model is that planetary migration in the inner solar system did not disrupt this final result and that the Fe content can help us figure out where an object formed.

Nebular gas carries the magnetic force in the protoplanetary disk. Metal-silicate segregation by solar magnetic forces is only effective before nebular gas dissipation (Kruss and Wurm, 2020; Wang et al., 2017). Mercury’s formation under reduced conditions in the presence of a gas disk with a strong magnetic field implies a $\tau_{\text{accretion}}$ age that is restricted to when a nebular envelope existed. Accretion in the presence of nebular gas is consistent with pebble accretion models of planetary formation, which may have contributed to the early formation of Mars and the iron meteorite parent bodies (Johansen et al., 2015). Therefore, a key implication of our model is an early formation age (~ 2 Myr) for Mercury, comparable to that of Mars (Dauphas and Chaussidon, 2011; Yoshizaki and McDonough, 2020a). Furthermore, our model does not require a giant impact event and partial loss of its silicate shell for the origin of Mercury’s large core (Benz et al., 2007; Asphaug and Reufer, 2014).

Incorporation of silicon, sulfur, and other elements into the Fe-Ni core of Mercury plays a minor role in establishing its size. Our model does not identify Mercury’s core composition; it remains a considerable unknown. We estimate a modest sulfur content for Mercury (2.5 ± 0.5 wt% (Methods) (cf., (Namur et al., 2016; Boujibar et al., 2019)) based on Mercury’s high bulk K/Th (6,000 to 8,000) (Nittler et al., 2018). The presence of silicon, sulfur, and other light elements, however, correspondingly lowers the solidus of the core and keeps it molten and convecting, thus providing the critically important conditions for dynamo action and magnetosphere generation.

The presence and size of a planetary metallic core depend on the redox environment of the protoplanetary disk and the planet’s mass fraction of accreted metal alloys, the latter of which is controlled by electromagnetic processing in the disk. A planet’s volatile element inventory (e.g., bulk sulfur content), coupled with the redox condition of core formation, controls the amount of light element in the core, which significantly lowers the core’s solidus and extends its molten-state lifetime. Collectively, these factors contribute to convection in a molten core and dynamo action. These attributes of our solar system would be equally applicable to exo-planetary systems. The generation of a planetary magnetosphere, which nurtures life, shapes a planet’s habitability. It is likely that life’s sustainability critically depends on being sited in the Goldilocks zone and having the right amount of metallic core, which contains an appropriate of a light element and is not cooling too fast.

Methods

Model description

The bulk composition of Mercury was defined to be consistent with its geodetic observables: mass, density, and MOI (moment of inertia) (Margot et al., 2018). Assuming a thermal gradient in the protoplanetary disk and the higher condensation temperature for forsterite (Mg_2SiO_4) versus enstatite ($\text{Mg}_2\text{Si}_2\text{O}_6$), then we predict a gradient in atomic Mg/Si (1.4) and Al/Si (0.12) values projecting from the values for Mars and Earth (Figure 2). The assumed Fe/Si (2.7) was established from a mass fraction of silicate to metal

to be consistent with Mercury’s uncompressed density (Figure 3), assuming proportions (40:53:7) and densities of silicates, metals, and sulfides (3,100, 7,100, and 4,600 kg m⁻³, respectively) as nominal values and with the metal alloy being a Fe-Ni-Si mixture. It is also likely that core-mantle differentiation add some fraction of silicon into the core under reducing conditions (Nittler et al., 2018). The atomic Ca/Al (0.73) and Fe/Ni (18.3) values are those seen in chondrites (Alexander, 2019a,b). The sulfur content was based on the planetary volatility trend established from Mercury’s measured K/Th value and an extrapolation to the condensation temperature, following the practice used in (McDonough and Sun, 1995; Yoshizaki and McDonough, 2020b). Ratios of alkali metals to refractory elements provide a constraint on a planet’s volatile element depletion trend, however, this simple model can be influenced by redox conditions and core formational processes. Finally, the oxygen content was set to make the total equal to 100%. This model establishes the bulk properties of Mercury, but it does not specify the distribution of elements between the core and mantle.

Data sources

Data sources for Figures 1 and 2 are as following: chondrites (Urey and Craig, 1953; Alexander, 2019a,b; McCall, 1968; Ivanova et al., 2008; Gosselin and Laul, 1990; Wasson and Kallemeyn, 1990; Bischoff et al., 1993); Mercury (this study); Earth (McDonough, 2014); Mars (Yoshizaki and McDonough, 2020b). For Figure 3, density of planetary bodies are from (Russell et al., 2012; Park et al., 2019; Sierks et al., 2011; Consolmagno et al., 2006; Macke et al., 2010, 2011; Britt and Consolmagno, 2003; Lewis, 1972; Stacey, 2005); heliocentric distances of chondrite parent bodies are from (Desch et al., 2018).

References

- Alexander, C.M.O., 2019a. Quantitative models for the elemental and isotopic fractionations in chondrites: The carbonaceous chondrites. *Geochimica et Cosmochimica Acta* 254, 277–309. doi:10.1016/j.gca.2019.02.008.
- Alexander, C.M.O., 2019b. Quantitative models for the elemental and isotopic fractionations in the chondrites: The non-carbonaceous chondrites. *Geochimica et Cosmochimica Acta* 254, 246–276. doi:10.1016/j.gca.2019.01.026.
- Asphaug, E., Reufer, A., 2014. Mercury and other iron-rich planetary bodies as relics of inefficient accretion. *Nature Geoscience* 7, 564. doi:10.1038/NCEO2189.
- Bai, X.N., 2015. Hall effect controlled gas dynamics in protoplanetary disks. II. Full 3D simulations toward the outer disk. *The Astrophysical Journal* 798, 84. doi:10.1088/0004-637X/798/2/84.
- Benz, W., Anic, A., Horner, J., Whitby, J., 2007. The Origin of Mercury. *Space Science Reviews* 132, 189–202. doi:10.1007/s11214-007-9284-1.
- Bischoff, A., Palme, H., Schultz, L., Weber, D., Weber, H.W., Spettel, B., 1993. Acfer 182 and paired samples, an iron-rich carbonaceous chondrite: Similarities with ALH85085 and relationship to CR chondrites. *Geochimica et Cosmochimica Acta* 57, 2631–2648. doi:10.1016/0016-7037(93)90422-S.
- Boujibar, A., Habermann, M., Richter, K., Ross, D.K., Pando, K., Richter, M., Chidester, B.A., Danielson, L.R., 2019. U, Th, and K partitioning between metal, silicate, and

- sulfide and implications for Mercury's structure, volatile content, and radioactive heat production. *American Mineralogist: Journal of Earth and Planetary Materials* 104, 1221–1237.
- Britt, D.T., Consolmagno, G.J.S.J., 2003. Stony meteorite porosities and densities: A review of the data through 2001. *Meteoritics & Planetary Science* 38, 1161–1180. doi:10.1111/j.1945-5100.2003.tb00305.x.
- Bryson, J.F.J., Weiss, B.P., Biersteker, J.B., King, A.J., Russell, S.S., 2020. Constraints on the Distances and Timescales of Solid Migration in the Early Solar System from Meteorite Magnetism. *The Astrophysical Journal* 896, 103. doi:10.3847/1538-4357/ab91ab.
- Connolly, Jr, H.C., Huss, G.R., Wasserburg, G.J., 2001. On the formation of Fe-Ni metal in Renazzo-like carbonaceous chondrites. *Geochimica et Cosmochimica Acta* 65, 4567–4588. doi:10.1016/S0016-7037(01)00749-9.
- Consolmagno, G.J., Macke, R.J., Rochette, P., Britt, D.T., Gattacceca, J., 2006. Density, magnetic susceptibility, and the characterization of ordinary chondrite falls and showers. *Meteoritics & Planetary Science* 41, 331–342. doi:10.1111/j.1945-5100.2006.tb00466.x.
- Dauphas, N., Chaussidon, M., 2011. A perspective from extinct radionuclides on a young stellar object: The Sun and its accretion disk. *Annual Review of Earth and Planetary Sciences* 39, 351–386. doi:10.1146/annurev-earth-040610-133428.
- Desch, S.J., Kalyaan, A., Alexander, C.M.O., 2018. The effect of Jupiter's formation on

- the distribution of refractory elements and inclusions in meteorites. The Astrophysical Journal Supplement Series 238, 11. doi:10.3847/1538-4365/aad95f.
- Dumoulin, C., Tobie, G., Verhoeven, O., Rosenblatt, P., Rambaux, N., 2017. Tidal constraints on the interior of Venus. Journal of Geophysical Research: Planets 122, 1338–1352. doi:10.1002/2016JE005249.
- Ebel, D.S., Alexander, C.M.O., 2011. Equilibrium condensation from chondritic porous IDP enriched vapor: Implications for Mercury and enstatite chondrite origins. Planetary and Space Science 59, 1888–1894. doi:10.1016/j.pss.2011.07.017.
- Fu, R.R., Kehayias, P., Weiss, B.P., Schrader, D.L., Bai, X.N., Simon, J.B., 2020. Weak magnetic fields in the outer solar nebula recorded in CR chondrites. Journal of Geophysical Research: Planets 125, e2019JE006260. doi:10.1029/2019JE006260.
- Gosselin, D.C., Laul, J.C., 1990. Chemical characterization of a unique chondrite: Allan Hills 85085. Meteoritics 25, 81–87. doi:10.1111/j.1945-5100.1990.tb00979.x.
- Harris, P.G., Tozer, D.C., 1967. Fractionation of iron in the Solar system. Nature 215, 1449–1451. doi:10.1038/2151449a0.
- Ivanova, M.A., Kononkova, N.N., Krot, A.N., Greenwood, R.C., Franchi, I.A., Verchovsky, A.B., Trierloff, M., Korochantseva, E.V., Brandstätter, F., 2008. The Isheyevo meteorite: Mineralogy, petrology, bulk chemistry, oxygen, nitrogen, carbon isotopic compositions, and ^{40}Ar - ^{39}Ar ages. Meteoritics & Planetary Science 43, 915–940. doi:10.1111/j.1945-5100.2008.tb01090.x.

- Johansen, A., Mac Low, M.M., Lacerda, P., Bizzarro, M., 2015. Growth of asteroids, planetary embryos, and Kuiper belt objects by chondrule accretion. *Science Advances* 1, e1500109. doi:10.1126/sciadv.1500109.
- Kruijer, T.S., Kleine, T., Borg, L.E., Brennecka, G.A., Irving, A.J., Bischoff, A., Agee, C.B., 2017. The early differentiation of Mars inferred from Hf–W chronometry. *Earth and Planetary Science Letters* 474, 345–354. doi:10.1016/j.epsl.2017.06.047.
- Kruss, M., Wurm, G., 2018. Seeding the Formation of Mercurys: An Iron-sensitive Bouncing Barrier in Disk Magnetic Fields. *The Astrophysical Journal* 869, 45. doi:10.3847/1538-4357/aaec78.
- Kruss, M., Wurm, G., 2020. Composition and size dependent sorting in preplanetary growth: seeding the formation of Mercury-like planets. *The Planetary Science Journal* 1, 23. doi:10.3847/PSJ/ab93c4.
- Larimer, J.W., Anders, E., 1970. Chemical fractionations in meteorites—III. Major element fractionations in chondrites. *Geochimica et Cosmochimica Acta* 34, 367–387. doi:10.1016/0016-7037(70)90112-2.
- Levy, E.H., 1978. Magnetic field in the primitive solar nebula. *Nature* 276, 481–481.
- Lewis, J.S., 1972. Metal/silicate fractionation in the solar system. *Earth and Planetary Science Letters* 15, 286–290. doi:10.1016/0012-821X(72)90174-4.
- Macke, R.J., Consolmagno, G.J., Britt, D.T., 2011. Density, porosity, and magnetic sus-

- ceptibility of carbonaceous chondrites. *Meteoritics & Planetary Science* 46, 1842–1862. doi:10.1111/j.1945-5100.2011.01298.x.
- Macke, R.J., Consolmagno, G.J., Britt, D.T., Hutson, M.L., 2010. Enstatite chondrite density, magnetic susceptibility, and porosity. *Meteoritics & Planetary Science* 45, 1513–1526.
- Margot, J.L., Hauck, I., Steven, A., Mazarico, E., Padovan, S., Peale, S.J., 2018. Mercury’s internal structure, in: Solomon, S.C., Nittler, L.R., Anderson, B.J. (Eds.), *Mercury The View after MESSENGER*. Cambridge University Press, pp. 85–113.
- McCall, G.J.H., 1968. The Bencubbin meteorite: Further details, including microscopic character of host material and two chondrite enclaves. *Mineralogical Magazine and Journal of the Mineralogical Society* 36, 726–739. doi:10.1180/minmag.1968.036.281.14.
- McDonough, W.F., 2014. Compositional model for the Earth’s core, in: Holland, H.D., Turekian, K.K. (Eds.), *Treatise on Geochemistry (Second Edition)*. Elsevier, Oxford. volume 3, pp. 559–577. doi:10.1016/B978-0-08-095975-7.00215-1.
- McDonough, W.F., Sun, S.s., 1995. The composition of the Earth. *Chemical Geology* 120, 223–253. doi:10.1016/0009-2541(94)00140-4.
- Namur, O., Charlier, B., Holtz, F., Cartier, C., McCammon, C., 2016. Sulfur solubility in reduced mafic silicate melts: Implications for the speciation and distribution of sulfur on Mercury. *Earth and Planetary Science Letters* 448, 102–114. doi:10.1016/j.epsl.2016.05.024.

- Nittler, L.R., Chabot, N.L., Grove, T.L., Peplowski, P.N., 2018. The Chemical Composition of Mercury, in: Solomon, S.C., Nittler, L.R., Anderson, B.J. (Eds.), *Mercury The View after MESSENGER*. Cambridge University Press, pp. 30–51.
- Park, R., Vaughan, A., Konopliv, A., Ermakov, A., Mastrodemos, N., Castillo-Rogez, J., Joy, S., Nathues, A., Polanskey, C., Rayman, M., Riedel, J., Raymond, C., Russell, C., Zuber, M., 2019. High-resolution shape model of Ceres from stereophotoclinometry using Dawn imaging data. *Icarus* 319, 812–827. doi:10.1016/j.icarus.2018.10.024.
- Russell, C.T., Raymond, C.A., Coradini, A., McSween, H.Y., Zuber, M.T., Nathues, A., De Sanctis, M.C., Jaumann, R., Konopliv, A.S., Preusker, F., et al., 2012. Dawn at Vesta: Testing the protoplanetary paradigm. *Science* 336, 684–686. doi:10.1126/science.1219381.
- Sierks, H., Lamy, P., Barbieri, C., Koschny, D., Rickman, H., Rodrigo, R., A'Hearn, M.F., Angrilli, F., Barucci, M.A., Bertaux, J.L., et al., 2011. Images of asteroid 21 Lutetia: a remnant planetesimal from the early Solar System. *science* 334, 487–490. doi:10.1126/science.1207325.
- Sohl, F., Schubert, G., 2015. Interior Structure, Composition, and Mineralogy of the Terrestrial Planets, in: Schubert, G. (Ed.), *Treatise on Geophysics (Second Edition)*. Elsevier, Oxford. volume 10, pp. 23 – 64. doi:10.1016/B978-0-444-53802-4.00166-4.
- Stacey, F.D., 2005. High pressure equations of state and planetary interiors. *Reports on Progress in Physics* 68, 341.

- Surkov, Y.A., Kirnozov, F.F., Glazov, V.N., Dunchenko, A.G., Tatsy, L.P., Sobornov, O.P., 1987. Uranium, thorium, and potassium in the Venusian rocks at the landing sites of Vega 1 and 2. *Journal of Geophysical Research: Solid Earth* 92, E537–E540. doi:10.1029/JB092iB04p0E537.
- Urey, H.C., Craig, H., 1953. The composition of the stone meteorites and the origin of the meteorites. *Geochimica et Cosmochimica Acta* 4, 36–82. doi:10.1016/0016-7037(53)90064-7.
- Wang, H., Weiss, B.P., Bai, X.N., Downey, B.G., Wang, J., Wang, J., Suavet, C., Fu, R.R., Zucolotto, M.E., 2017. Lifetime of the solar nebula constrained by meteorite paleomagnetism. *Science* 355, 623–627. doi:10.1126/science.aaf5043.
- Wardle, M., 2007. Magnetic fields in protoplanetary disks. *Astrophysics and Space Science* 311, 35–45.
- Warren, P.H., 2011. Stable-isotopic anomalies and the accretionary assemblage of the Earth and Mars: A subordinate role for carbonaceous chondrites. *Earth and Planetary Science Letters* 311, 93–100. doi:10.1016/j.epsl.2011.08.047.
- Wasson, J.T., Kallemeyn, G.W., 1990. Allan Hills 85085: A subchondritic meteorite of mixed nebular and regolithic heritage. *Earth and Planetary Science Letters* 101, 148–161. doi:10.1016/0012-821X(90)90150-V.
- Weidenschilling, S.J., 1978. Iron/silicate fractionation and the origin of Mercury. *Icarus* 35, 99–111. doi:10.1016/0019-1035(78)90064-7.

Wurm, G., Tieloff, M., Rauer, H., 2013. Photophoretic separation of metals and silicates: The formation of Mercury-like planets and metal depletion in chondrites. *The Astrophysical Journal* 769, 78. doi:10.1088/0004-637X/769/1/78.

Yoshizaki, T., McDonough, W.F., 2020a. Earth and mars—distinct inner solar system products. arXiv preprint arXiv:2006.11051 .

Yoshizaki, T., McDonough, W.F., 2020b. The composition of Mars. *Geochimica et Cosmochimica Acta* 273, 137–162. doi:10.1016/j.gca.2020.01.011.

Acknowledgments

We thank many our colleagues who have listened to various versions of this project and given helpful comments. WFM gratefully acknowledges NSF support (EAR1650365). TY acknowledges supports from the Japanese Society for the Promotion of Science (JP18J20708) and the GP-EES and DIARE programs.

Author contributions

WFM and TY proposed and conceived various portions of this study and together calculated the compositional models. The manuscript was written by WFM, with edits, discussions, and revisions by TY & WFM. Both authors read and approved the final manuscript.

Competing interests

The authors declare no competing interests.

Data and materials availability

Correspondence and requests for materials should be addressed to WFM.

Supplementary information

Supplementary information is available for this paper.

Table 1: **Composition of the terrestrial planets.**

Atomic%	Mercury (see Methods)	Earth & Venus (McDonough, 2014)	Mars (Yoshizaki and McDonough, 2020b)	CI chondrite (volatile-free) (Alexander, 2019a)
O	36.8	49.0	55.3	48.2
Mg	15.6	16.7	15.3	15.1
Si	11.0	15.1	15.1	14.7
Fe	30.0	15.1	10.3	12.8
Ni	1.64	0.82	0.57	0.70
Al	1.38	1.56	1.41	1.20
Ca	1.00	1.13	1.03	0.88
S	2.49	0.52	0.92	6.43
Fe/Si	2.72	1.00	0.69	0.87
Fe/Al	21.8	9.7	7.3	10.6
Fe/O	0.82	0.31	0.19	0.26
Mg/Si	1.42	1.11	1.02	1.03
Al/Si	0.12	0.10	0.09	0.08
Mean Z	15.4	12.7	11.8	12.6
Mass%	Mercury	Earth & Venus	Mars	CI (volatile-free)
O	18.3	29.7	36.3	29.1
Mg	11.8	15.4	15.3	13.9
Si	9.65	16.1	17.4	15.6
Fe	52.3	32.0	27.3	26.9
Ni	3.00	1.82	1.36	1.54
Al	1.16	1.59	1.56	1.22
Ca	1.25	1.71	1.69	1.33
S	2.50	0.64	1.21	7.78

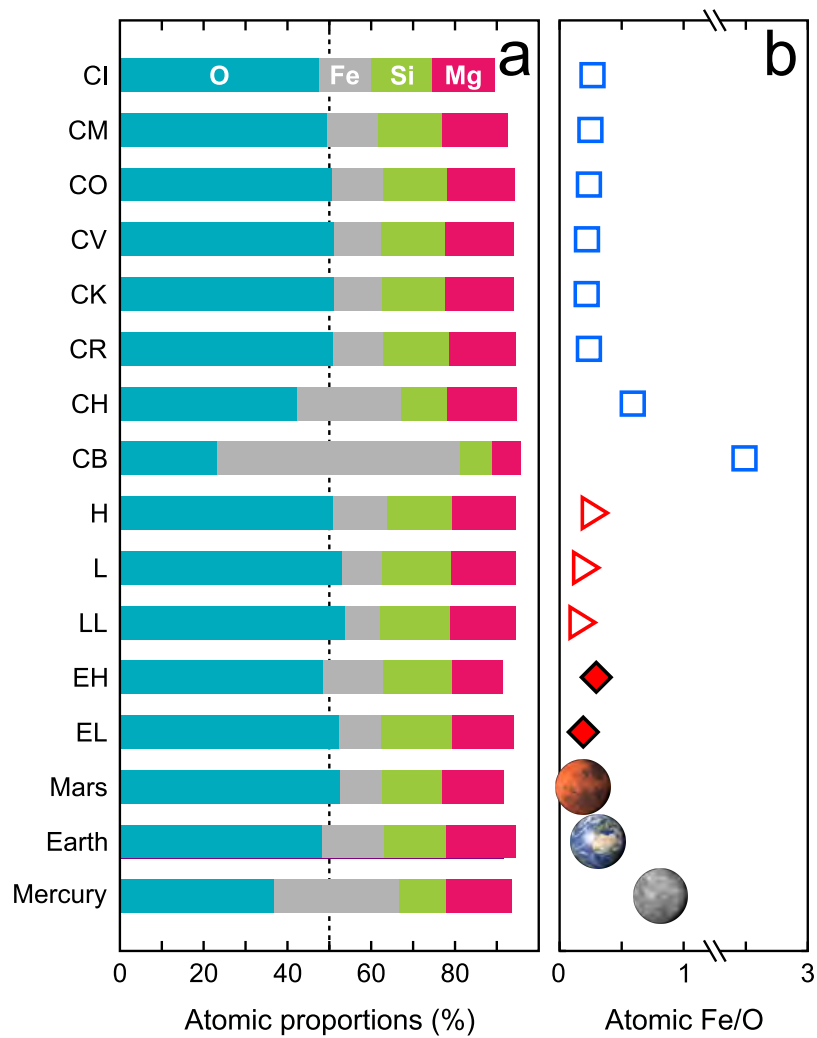


Figure 1: (a) Atomic abundances of major elements and (b) Fe/O values in the solar system bodies. Data sources are given in supplementary materials.

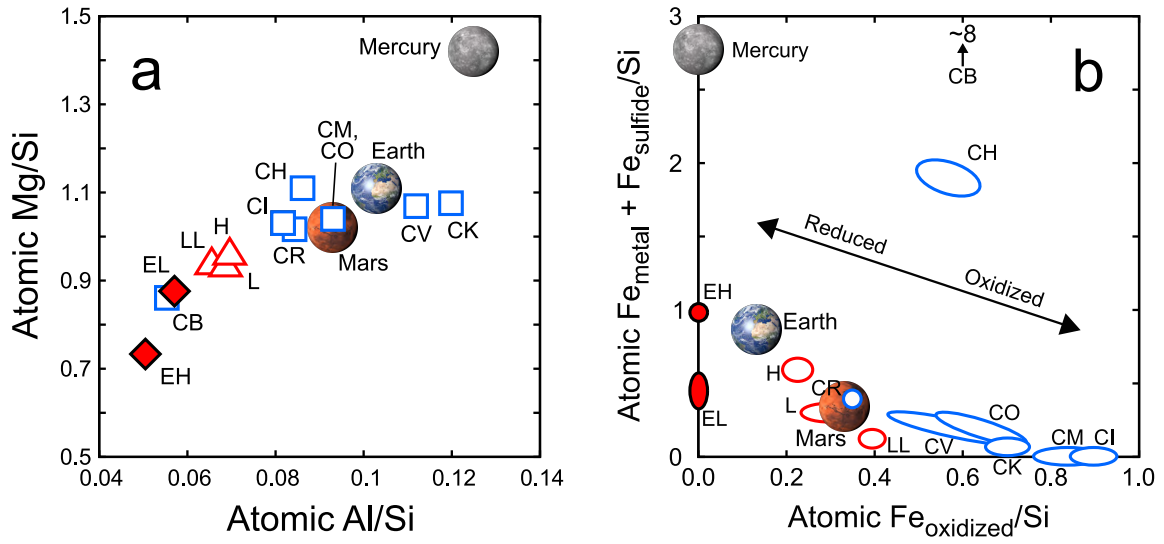


Figure 2: **Ratios of major cations in the terrestrial planets and chondrites.** (a) Magnesium/Si versus Al/Si. (b) Abundances of reduced (metal and sulfide) and oxidized Fe normalized to Si. Data sources are given in supplementary materials. Red symbols identify the inner solar system, NC chondrites; see text for details.

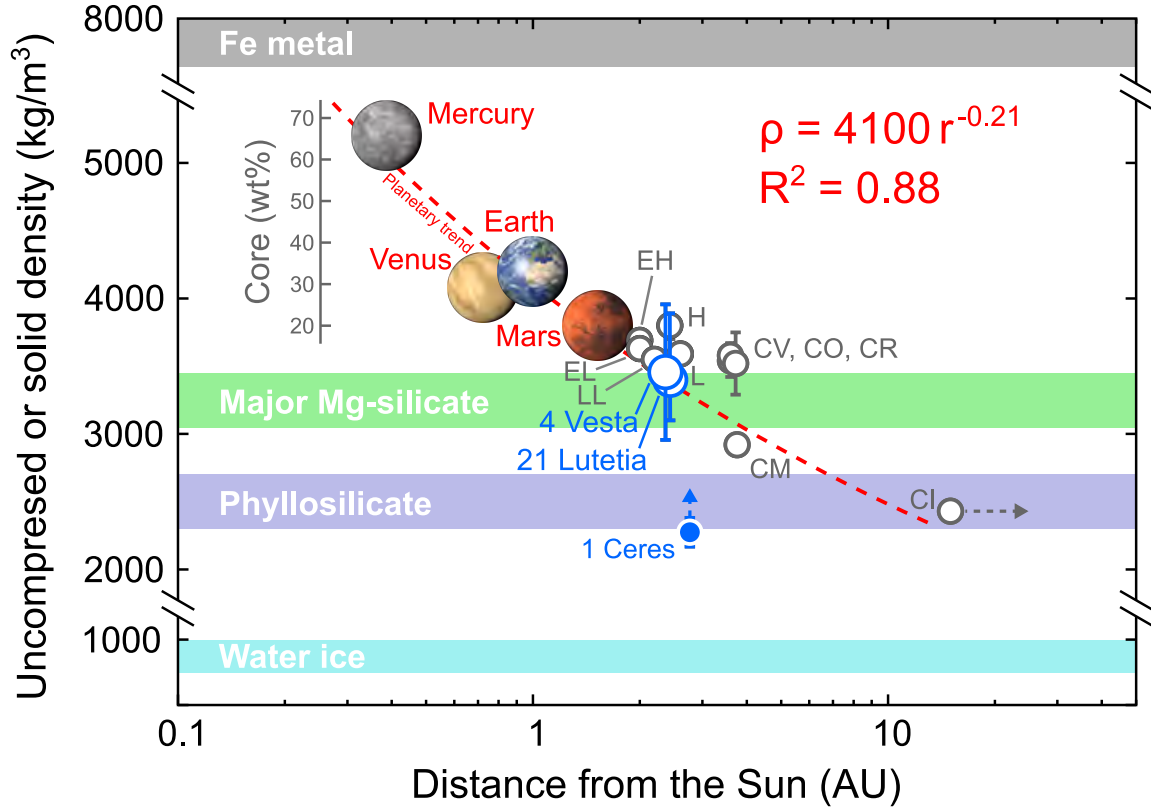
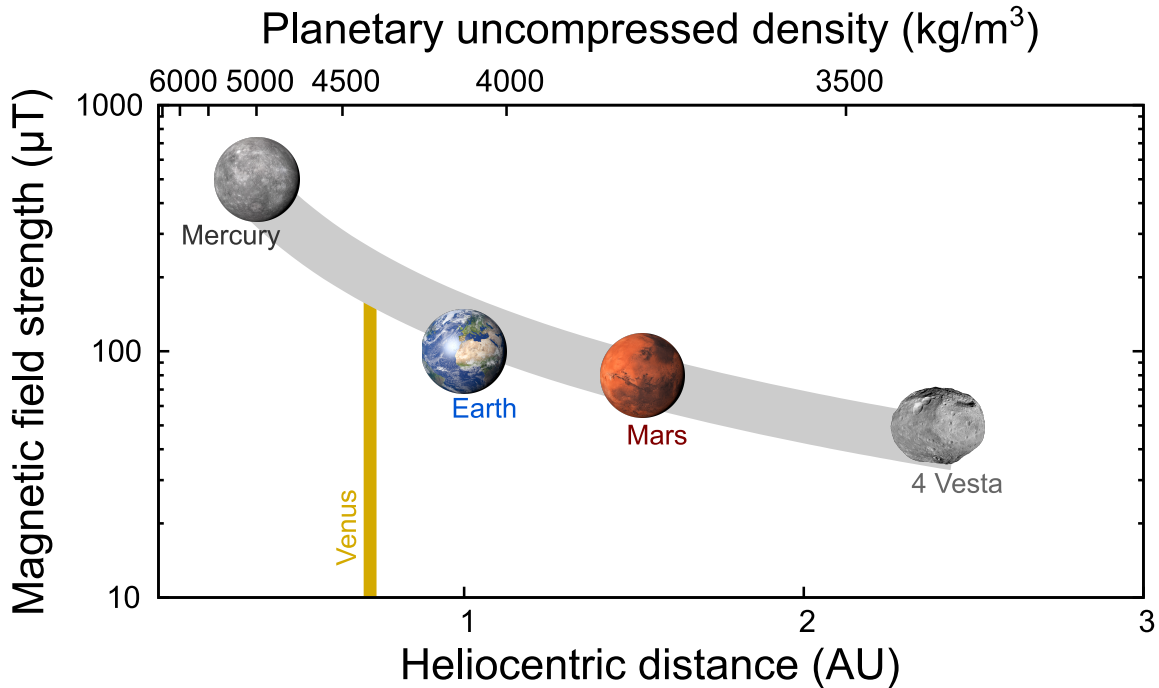


Figure 3: **Density of the solar system bodies.** Uncompressed and solid densities are shown for terrestrial planets and chondrites (grey), respectively. Bulk planetary densities are shown for asteroids (blue). For 1 Ceres, its bulk density is a lower limit of its solid density, given its high ice abundance and porosity. The red line shows a fit curve for the planets ($\rho = 4,100r^{-0.21}$). Data sources are given in supplementary materials.

Supplementary information



Supplementary Figure 1: A simple Biot-Savart type model for the average magnetic field strength versus accretion position of the terrestrial planets in the protoplanetary disk. A top x-axis shows the correlation between uncompressed density and heliocentric distance. See text for details and data. A prediction for Venus is shown with a bar; its uncompressed density is $4,100 \text{ kg m}^{-3}$ (Lewis, 1972; Stacey, 2005).